(Received 16 October 2024, Accepted 29 November 2024, Scheduled 8 December 2024)

AI-Tuned Metantenna Antenna for Fifth Generation & Beyond Communication Applications

Bikash Ranjan Behera* and Harikrishna Paik

Department of Electronics and Communication Engineering
Vel Tech Rangarajan Dr. Sagunthala R&D Institute of Science and Technology (Deemed-To-Be University)
Chennai, Tamil Nadu 600062, India

ABSTRACT: For the purpose of fifth-generation and beyond communication applications, broadband circularly polarized (CP) & high gain AI-tuned metantenna operating in the 5 GHz band is presented in this article. So, a linearly polarized (LP) printed monopole antenna is being taken into consideration in the initial stage. To initiate CP from LP, a metallic strip that functions as a dynamic switching mechanism is utilized to short one of the parasitic conducting strips (PCSs) with partial ground plane. The objective is to enhance the impedance (IBW) and axial bandwidths (ARBWs) as well as the antenna gain in order to make it a suitable candidate for ambient RF energy harvesting/wireless energy harvesting application. To achieve this, AI-tuned metasurface is placed below the monopole radiator at a height of $0.33\lambda_o$. With a measured 49.84% IBW, 18.95% ARBW, CP gain > 8 dBic, antenna efficiency $> 70\%$, fabricated on an FR-4 substrate with $1.33\lambda_o \times 0.9\lambda_o \times 0.02\lambda_o$, it is better for the technological deployments in current wireless technology, assuring resilience in networks. The transformation is brought by the utilization of metasurfaces offering customized, effective, and typical control of electromagnetic waves keeping with the desired frequency conditions.

1. INTRODUCTION

Compared to the communication systems that are now in existences, wireless communications rapidly progressing toward the next generation, i.e., fifth-generation and beyond, have significant expectation for data speeds, dependability, coverage, capacity, efficiency, connectivity, and latency. Through the enhancement of capabilities of wireless systems, antennas, as distinctive and forward-thinking passive devices, play a vital part in designing the future of wireless communications. By considering the current circumstances, there is urgent need for research that is geared toward the development of harnessing energy with the help of ambient signals. Thus, when low power embedded devices are taken into consideration, radio frequency (RF) energy harvesting through the utilization of electromagnetic spectrums has emerged as means of reducing costs with minimal periodic maintenance [1]. It is in reference with the application of RF energies in the real-time scenario. The reason for this is that it requires us to interact with the EM waves that are all around us; in this context, radio frequency front-ends are considered a crucial component of the process [2]. It is quite possible to observe their efficacy by making use of the properties of CP in order to achieve better signal matching [3]. The first and most important step is to ensure that the incoming signals from operating frequency bands, such as mobile communication bands, are received correctly, regardless of the direction in which the antenna is pointing [3]. The selection of the front-ends is crucial because of low profile, easy analysis, wide bandwidth, good radiation efficiency, satisfactory pattern, good time domain utility, & sensitivity towards Federal Communications Commission (FCC) emission limitation [4]. For this reason, printed monopole [5] was chosen with the motive of working towards improving the capabilities of wireless systems [6–9].

Consequently, there is a necessity for single antenna element that possesses qualities, notably the capability of CP. For the purpose of developing the CP antenna, techniques like vias [10] and metasurfaces [11–23] are applied. But, when it comes to the requirements for efficient polarization system, one of the most significant requirements is to get broadband CP characteristics in terms of bandwidths and gain. This particular type of analogy was not described in [10–23] and continues to be a great challenge to the researchers working in this area of interest [24], particularly when it comes to the implementation of metasurface layers that are not well defined through the application of AI approaches. So, the technique known as surrogate model-assisted differential evolution (SADEA) [25, 26] was employed for the purpose of optimizing parameters to improve fundamental performances [24–31], from the consideration of various needs. However, its application towards the optimization of engineered metasurfaces has not yet been reported in the literature, critical to CP metantenna towards its enhancement of bandwidth and gain. By using metallic short & incorporation of SADEA-driven metasurface layer of uniform with symmetrically placed unit cells, the broadband characteristics of CP and broadside directional pattern are achieved. Prior to it, comprehensive analogy of CP is proposed through the interpretation of computational electromagnetism (CEM) in the form of gain-bandwidth product (GBPR).

* Corresponding author: Bikash Ranjan Behera (drbikash@veltech.edu.in).

2. DESIGN FRAMEWORK OF A METANTENNA: CEM DESIGNING AND USAGE OF AI-TUNED SADEA APPROACH

Initially, a $\lambda_o/4$ LP monopole antenna with partial ground plane is designed for Wi-MAX/WLAN applications. We observe that the input impedance of a simple rectangular monopole is resistive of a value around 50-Ω at the center resonant frequency at which the antenna length is $\lambda_o/4$, as λ_o is the wavelength. At the frequencies, below the resonance frequency, the printed monopole becomes capacitive, while at the higher frequencies, where the length of the monopole is larger than $\lambda_o/4$, the input impedance is inductive. Thus, in this manner, one of the initial geometrical antenna parameters, Y-shaped monopole arm length, is chosen that suits our prospects. Figure 1 illustrates the schematics of the metantenna that has been designed on a low-cost FR-4 substrate. In order to address trade-offs (i.e., CP bandwidth and gain), we expanded the ground plane by incorporating 2 additional conducting strips. These strips have dimensions of 21.6 mm (length) and 1.84 mm (width), which are

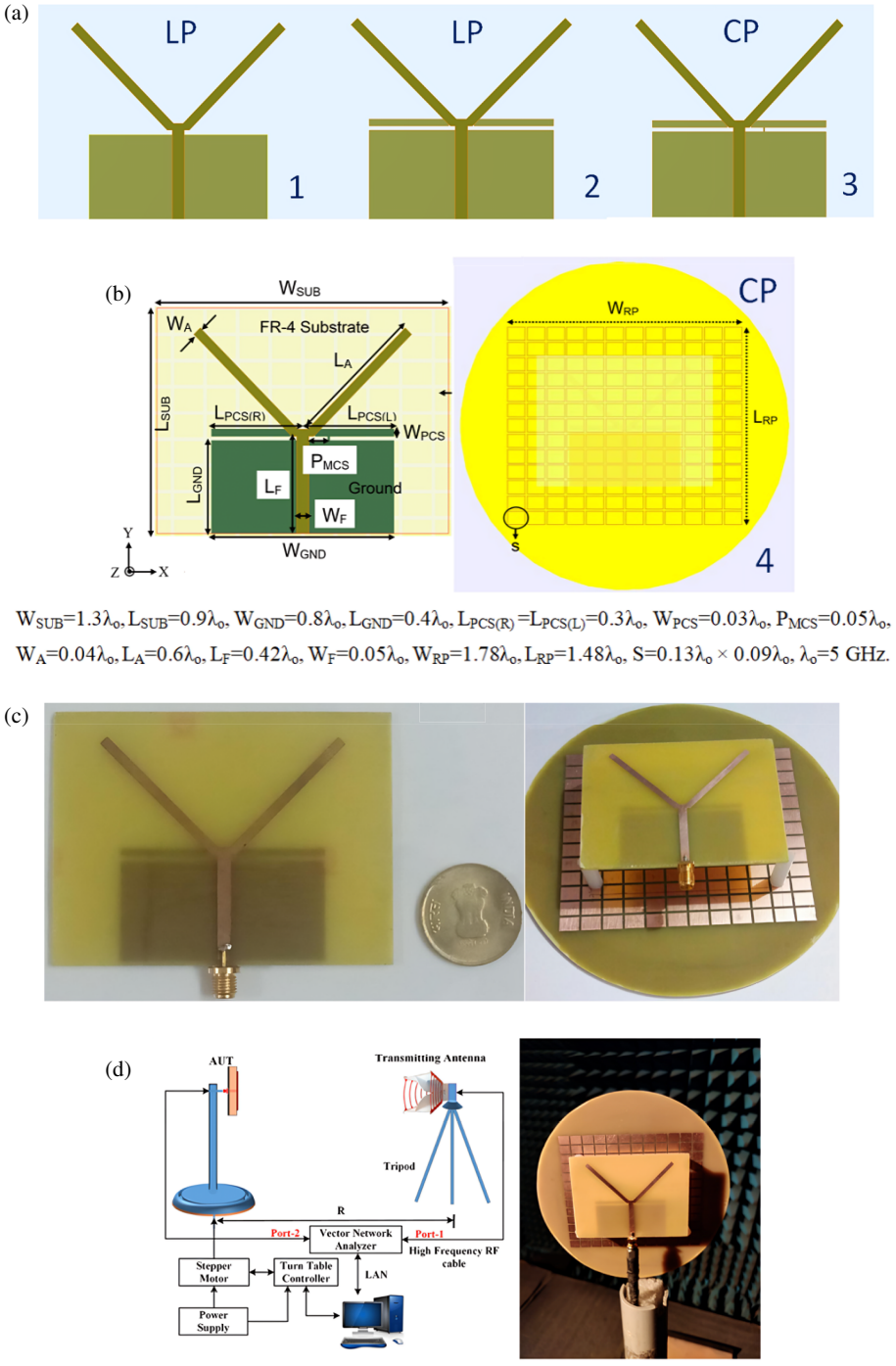

$W_{SUB}=1.3\lambda_o$, $L_{SUB}=0.9\lambda_o$, $W_{GND}=0.8\lambda_o$, $L_{GND}=0.4\lambda_o$, $L_{PCS(R)}=L_{PCS(L)}=0.3\lambda_o$, $W_{PCS}=0.03\lambda_o$, $P_{MCS}=0.05\lambda_o$, $W_A=0.04\lambda_o$, $L_A=0.6\lambda_o$, $L_F=0.42\lambda_o$, $W_F=0.05\lambda_o$, $W_{RP}=1.78\lambda_o$, $L_{RP}=1.48\lambda_o$, $S=0.13\lambda_o \times 0.09\lambda_o$, $\lambda_o=5$ GHz.

FIGURE 1. (a)–(d) Evolution (stages), schematics of the metantenna along with its fabricated prototype.

TABLE 1. Dimensions of the metantenna for ambient RF energy harvesting/wireless power transmission.

Parameters	Range	SADEA Optimized (Stage-4)
Size of The Unit Cells	$0.1\lambda_o$-$0.2\lambda_o \times 0.005\lambda_o$-$0.015\lambda_o$	$0.15\lambda_o \times 0.01\lambda_o$
Intermediate Gap Between The Unit Cells	$0.012\lambda_o$-$0.022\lambda_o$	$0.016\lambda_o$

separated from the upper faces of the partial ground plane by the offset of 1.16 mm. The interaction that exists in between the partial ground and parasitic conducting strip, PCS(L), serves as a vital determinant to determine the desired CP characteristics, considering from application perspective. This communication can be established through the connection of partial ground plane and PCS(L), utilizing the metallic strip. So, the application of SADEA-tuned metasurface contributes to an accomplishment of broadband CP with a manipulation towards focussed strong directional pattern with the elevated front-to-back ratio (FBR) and 3-dB angular beamwidth.

Hence, we elaborate the process of incorporating SADEA-tuned metasurface in the scenario of proposed metantenna for the ambient RF energy harvesting/wireless power transmission. Utilizing MATLAB Antenna Toolbox™, users are granted access to a range of functions and applications that are utilized for the purpose of designing, analyzing, and visualizing the microwave ends. Therefore, the unit cells [6], a key component of artificially engineered metasurfaces, are included among the component elements. So, the question that needs to be answered is whether it is possible to generate the outcomes [24] by making usage of discrete 3D forms, arbitrary planar structures, and/or parametrically determined parts. The fact that it makes use of an EM solver makes it equally capable of computing all of the desired characteristics in order to carry out final verification, as the methods of moments (MoM) do. To optimize the designs in most efficient manner, it enables the manual optimization. SADEA is a method that is used to optimize designs based on the fundamental principles of AI. Machine learning & evolutionary computation is the theoretical foundation [24–31] upon which it is framed.

To construct a surrogate model, statistical learning approaches are used when doing the global optimization, which is carried out with the assistance of SADEA. Consequently, in the context of the surrogate model-assisted optimization approach, it is of the utmost importance that the procedures that are used to make the surrogate modeling & its optimization work together in successful manner. Additionally, concepts borrowed from evolutionary search framework that takes surrogate models into consideration have been included into SADEA. Both the search engines that SADEA employs are referred to as the differential evolution (DE), and the machine learning technique that is utilized for the surrogate modeling makes use of a Gaussian process (GP) [30, 31]. When it comes to the design of metantenna, it seems that SADEA optimization is only used in extremely exceptional situation, being quite uncommon in the literature when it comes to the optimization of metasurfaces. Through the use of MATLAB R2022b platform, the process of optimizing a metasurface layer to enhance the performance of CP metantenna is taken into consideration for ambient RF energy harvesting/wireless power transmission application. In Figures 2(a) and (b), comprehensive description concerning the procedure & insights involved and its implementation is shown, right from designing to optimization.

The objective of the optimization is to obtain improvement in the outcomes of: (a) maximizing operating bandwidth and (b) limiting the area of occupation for a proposed metasurface layer (i.e., dimensions). This is accomplished through the utilization of the AI-tuned SADEA method. When the trade-offs are taken into consideration from a point of view of the application, significant observation is made during this analysis. It plays a significant part in ensuring that the antenna's performance is maintained, and in continuation with a motive of attaining improved outcomes, execution is performed for the metasurface reflector (for optimizing size of grid-slotted sub-patches cells, intermediate gap, and its overall size) placed at a height of $0.33\lambda_o$ below of it. The optimized dimension is shown in Table 1, which will be used in the process of experimental validations.

To further analyze the situation, it is important to note that Equation (1) has additional parameters that play a role in deciding the dimensions of effective gap ($h_{\text{air}-\text{gap}}$) between the radiator and SADEA-driven metasurface layer. It includes the parameters such as thickness of the substrate (h_{sub}), relative permittivity of the substrate (ε_r), and its operating wavelength (λ_o). The simulated $h_{\text{air}-\text{gap}}$ as 20 mm and the theoretical $h_{\text{air}-\text{gap}}$ as 20.85 mm are determined. As said above, the final mathematical formulation is presented in this study, which is used in the scenario of deploying the metasurface reflectors, in order to begin the process of examining placement in relation to the CP radiator, by simply approximating $h_{\text{air}-\text{gap}}$ using the analytical approach as given below:

$$h_{\text{air}-\text{gap}} = 0.42\lambda_0 - h_{\text{sub}}\sqrt{\varepsilon_r} \tag{1}$$

So, compared to the previous value of 2.35 dBic (stage-3, without metasurface layer), the average CP gain increases by a factor of 3.65, reaching 8.58 dBic. Moreover, the metantenna's IBW grows by a factor of 1.1 times, going from 2.11 GHz to 2.32 GHz, and the ARBW increases by a factor of 1.89 times, going from 0.46 GHz to 0.87 GHz (stage-4), respectively. Enhancement in both of them is too crucial. The attainment of such antenna performances is motivated by a geometric understanding, since the goal of the development is to achieve the performance trade-offs with a metantenna. So, it has been demonstrated that metasurface unit cells are proposed to concentrate radiation fields towards occurrence of quasi-TM_{30}

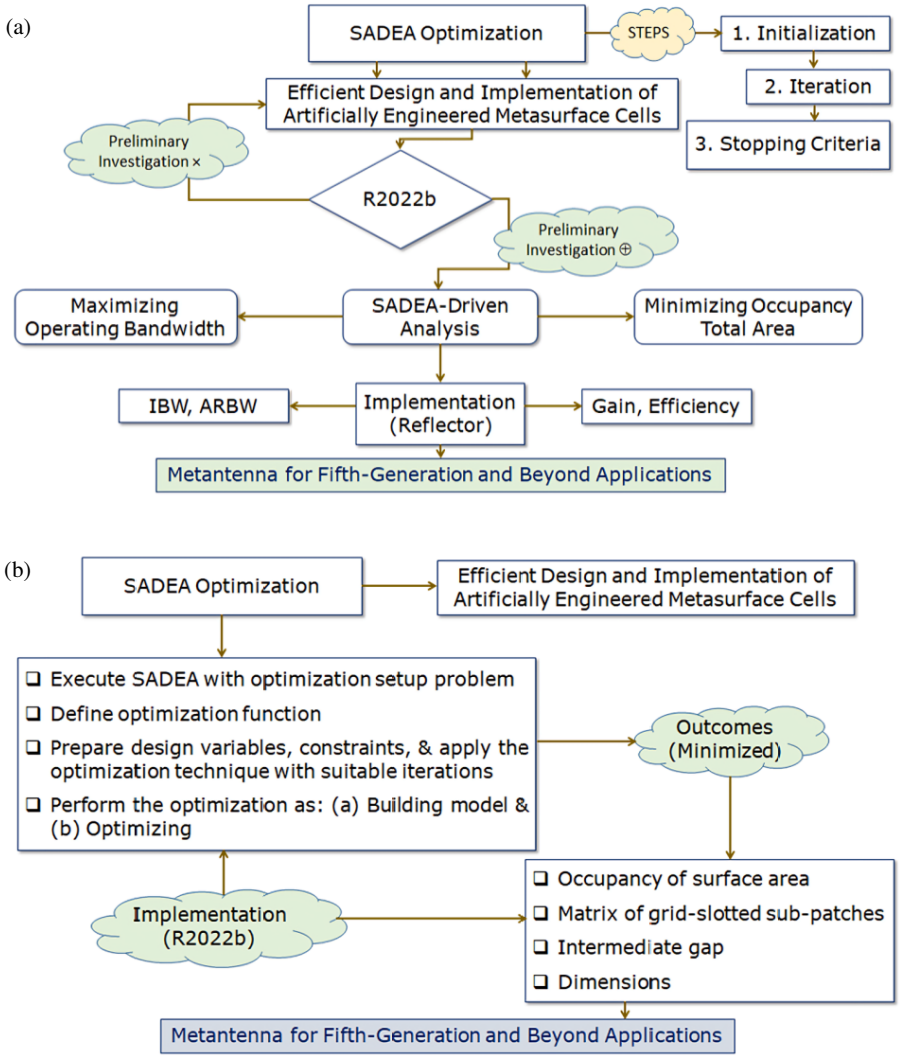

FIGURE 2. Insights to the procedure (SADEA): (a), (b) Process and its implementation for metantenna.

modes (transformation of TM_{10} to TM_{30} modes) by utilizing Finite Integration Technique (FIT). In turn, it leads to a more uniform E-field distribution and ultimately improved impedance performance at 5 GHz. The unit cells expressed in the form of grid-slotted sub-patches is the source of higher modes [32] as depicted in the Figure 3. The impedance matching is improved through the use of SADEA. It is accomplished by the gaps that exist between sub-patches, and gaps allow radiation to behave constructively. Metasurface (MTS) has the ability to manipulate the behaviour of EM waves as presented in Figure 4.

Further, the layers of inductive and capacitive components are piled one on top of the other to form the MTS layer. It is then coupled to the inductive unit cells that are situated on layer L_2, and capacitive C_1 separates the MTS. L_1 serves as exterior radiating border. The inductance L_3 layer then creates connections within antenna, and due to the overall inductances it makes contribution to the process of determining the influence of total surface impedances. Here, $e_q = Z_a||Z_b$ is the formula that is used to determine an equivalent surface impedance, and Equations (2) and (3) provide a frequency dependency w.r.t. inductive and capacitive components [35, 36]. So, there is a representation in correlation with frequency as follows:

$$\eta_{eq} = \frac{j\omega L_3\left(1-\omega^2 L_1C_1-\omega^2 L_2C_1\right)}{1-\omega^2 L_1C_1-\omega^2 L_2C_1-\omega^2 L_3C_1} \tag{2}$$

$$f_R = \frac{1}{2\pi\sqrt{\left(L_1+L_2+L_3\right)C_1}} \tag{3}$$

3. CONCEPTION OF CIRCULAR POLARIZATION (CP): UNDERSTANDING THE CONCEPT & ITS ANALYSIS ON ANTENNAS

A better understanding of CP has been given by different responses towards CP analysis shown in Figure 5. The first and most basic way to look at how CP behaves is to look at how surface currents are distributed (I). So, there are no parasitic conducting strips (PCSs) present at stage-2, and it is not possible to establish connection with the partial ground planes. Unlike the vertical surface currents on the monopole arm, the induced

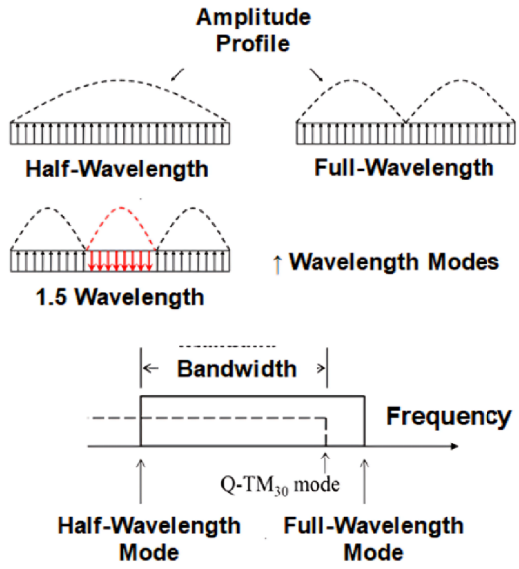

FIGURE 3. Transformation of half-wavelength to full-wavelength modes for a SADEA-tuned metasurface.

surface currents on the horizontal spaces of the partial ground plane flow in their quite opposite way, as if they were canceling each other. An LP wave is making because of that. When the metallic strip connects with one of the parasitic conducting strips, PCS(L) to the partial ground plane in stage-3, the surface currents on the PCS(L) and partial ground plane are rearranged, so that the currents on the upper edges of the PCS(L) and the lower edge of the partial ground plane run in the same direction. Hence, this creates horizontal surface current. The viability of CP is contingent upon the presence of both horizontal and vertical components, referring to horizontal and vertical currents [6, 33], suggesting that the CP can be explained as through the component of CEM, highlighted precisely in Figure 5(a).

Analyzing the CP using the distribution of the electric field (II) is performed. PCS(L) is connected to the partial ground plane through the metallic strip and allows the metantenna to achieve left hand circular polarization (LHCP) in the $+z$ direction, which is outward in nature. At 5 GHz, the phase of electric field vectors shifts from 0° to 90° which indicates that they rotate in anticlockwise (ACW) direction. So, the existence of orthogonal change in the pattern of the electric field ensures LHCP and is confirmed in Figure 5(b). When the magnitudes of electric fields move in anticlockwise manner from 90° to 360°, a similar tendency is observed. So, the right-hand thumb rule is frequently used to characterize the characteristics, and plane wave equation is used. Assuming that x and y are linearly polarized waves with complex amplitudes, E_x and E_y, change in space & time, the total electric fields is expressed as follows (mathematical representation, CEM):

$$\vec{E}(z) = (E_x\hat{x} + E_y\hat{y})\, e^{j\beta z} \tag{4}$$

In the next part, we can express the total electric fields as amplitudes and phases:

$$\begin{aligned}\vec{E}(z,t) &= \left(E_{x_0}e^{j\omega t}\hat{x} + E_{y_0}e^{j\omega t}\hat{y}\right) e^{-j\beta z} \\ &= E_{x_0}e^{j(\omega t-\beta z)}\hat{x} + E_{y_0}e^{j(\omega t-\beta z)}\hat{y} \end{aligned} \tag{5}$$

When we isolate the real term from Equation (5), accounting for the time dependence, we obtain:

$$\vec{E}(z,t) = E_{x_0}\cos(\omega t-\beta z)\hat{x} + E_{y_0}\cos(\omega t-\beta z)\hat{y} \tag{6}$$

CP analysis takes into account parameters such as the horizontal and vertical field components in 90° phase quadrature and having equal amplitude, for which they can be again realized as:

$$\begin{aligned}\vec{E}_{\text{LHCP}}(z,t) &= E_0\cos(\omega t-\beta z)\hat{x} + E_0 e^{\frac{j\pi}{2}}\cos(\omega t-\beta z)\hat{y} \\ &= E_0\cos(\omega t-\beta z)\hat{x} + E_0 j\cos(\omega t-\beta z)\hat{y} \\ &= E_0\cos(\omega t-\beta z)\hat{x} + E_0\cos\left(\omega t-\beta z+\frac{\pi}{2}\right)\hat{y}\end{aligned}$$

At $z = 0$, the above equation is changed into:

$$\vec{E}_{\text{LHCP}}(0,t) = E_0\cos(\omega t)\hat{x} + E_0\cos\left(\omega t+\frac{\pi}{2}\right)\hat{y} \tag{7}$$

In Equation (7), by taking the propagation direction into account, CP analysis for the LHCP is pursued.

In the realm of CP analysis, the normalized radiation pattern (III) is studied. Hence, the relative power at the intended operating frequency bands (3.5/5 GHz) is discovered to have a correlation with particular correlation. At 5 GHz, the metantenna exhibits LHCP, as LHCP gain is stronger than the right hand circular polarization (RHCP) gain, as shown in Figure 5(c). The maximum gain at LHCP is 3.58 dBic, while the highest gain at RHCP is 3.39 dBic. Also, the dominance's of CP components is evaluated based on the conditions shown in Equations (8) and (9) and highlighted in Figure 5(d). Hence, investigating the CP's behavioral explanation that was reported has made substantial usages of I, II, and III methods. The amplitude & phase responses (IV) highlighted in Figure 5(e) are finally presented in the more effective manner, which allows the CP characteristics to be comprehended.

$$\vec{E}_{\text{LHCP}} = \frac{1}{\sqrt{2}}(E_x + jE_y) \tag{8}$$

$$\vec{E}_{\text{RHCP}} = \frac{1}{\sqrt{2}}(E_x - jE_y) \tag{9}$$

Here, the authors provide the intuition on the CP with different characteristics that is predicated on a CEM at the same time. It is illustrated in addition to the physical insights as well. Thus, with the purpose of tackling applications that are inspired by the fifth-generation & beyond application, comprehensive design is offered for the wide-scale solution, when CP properties are taken into consideration. Methods (I) to (IV) are part of computational electromagnetism (CEM), which is an important task force, when it comes for the scope of evaluating, designing, & optimizing systems, especially for the antennas that make use of the CP condition.

Also, gain-bandwidth product (GBPR) is essential for microwave devices although the bandwidth(s) and gain trade-offs are important in antenna design. To optimize performance

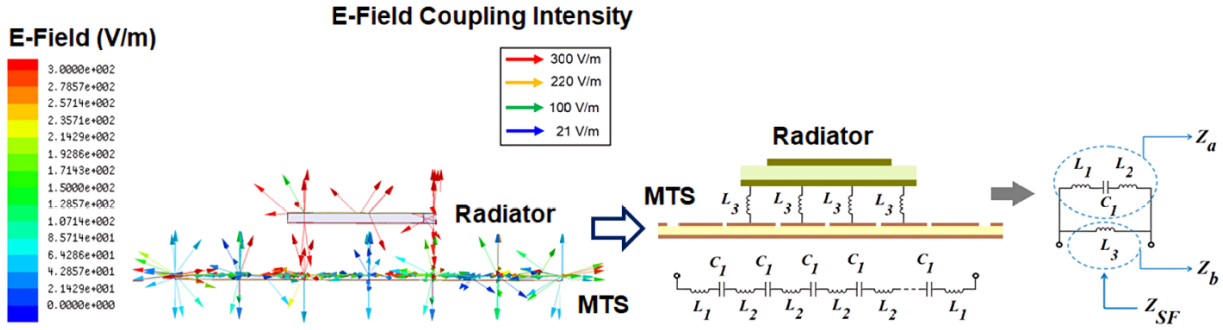

FIGURE 4. Understanding the electric field coupling intensities affecting the performance of CP metantenna.

TABLE 2. An analogy comparing the metantenna and CP metamaterial antennas in [10–23], when it comes to GBPR (Performance Trade-offs: IBW $>$ 45%, ARBW $>$ 18%, CP antenna gain $>$ 8 dBic, C_1 and C_2 $>$ 1.8).

Ref.	IBW	ARBW	3-dB$^{avg.}$	3-dB^{peak}	C_1	C_2	Trade-offs	AI-Used
[10]	7.29%	5.5%	6.5 dBic	7.1 dBic	0.35	0.39	‡	×
[11]	16%	10%	5.5 dBic	6.6 dBic	0.55	0.67	‡	×
[12]	22.6%	14.3%	4.2 dBic	4.8 dBic	0.61	0.68	‡	×
[13]	33.7%	16.5%	5.8 dBic	5.8 dBic	0.95	0.95	‡	×
[14]	34.3%	18.69%	5.1 dBic	6.1 dBic	0.95	1.14	‡	×
[15]	16.8%	18%	4.8 dBic	6.8 dBic	0.86	1.22	‡	×
[16]	29.41%	9.05%	6.3 dBic	6.3 dBic	0.57	0.57	‡	×
[17]	16.36%	11.93%	5.6 dBic	5.9 dBic	0.67	0.71	‡	×
[18]	33.6%	18.2%	7.6 dBic	7.9 dBic	1.38	1.44	‡	×
[19]	20.5%	15.5%	4.2 dBic	4.2 dBic	0.65	0.65	‡	×
[20]	39.25%	17.77%	6.8 dBic	6.8 dBic	1.21	1.21	‡	×
[21]	20.6%	17.4%	8.1 dBic	8.3 dBic	1.39	1.44	‡	×
[22]	1.55%	1.05%	7.8 dBic	8.2 dBic	0.07	0.08	‡	×
[23]	25.17%	17.42%	7.5 dBic	7.5 dBic	1.31	1.31	‡	×
Stage-1	19.78%	×	×	×	×	×	‡	×
Stage-2	13.45%	×	×	×	×	×	‡	×
Stage-3	45.46%	10.38%	2.35 dBic	2.35 dBic	0.24	0.24	‡	×
Stage-4	**49.84%**	**18.95%**	**8.55 dBic**	**8.85 dBic**	**1.92**	**1.98**	**Attained**	**Implemented**

***Nomenclature Used in the Table 2** ‡: Less Than Performance Trade-offs and ×: Not Implemented

across the intended band, designer must consider them. Understanding how bandwidth and gain interact helps choose design systems that fulfill needs, GBPR [6], Equation (10) represents that 3-dB bandwidth & 3-dB gain as the function of the criterion:

$$C = F\left(\mathrm{BW}_{\text{3-dB}}, G_{\text{3-dB}}\right) \tag{10}$$

Equation (10) can be written in the product form as:

$$C = \mathrm{BW}_{\text{3-dB}} \times G_{\text{3-dB}} \tag{11}$$

Representing Equation (11) in the form of a ratio, it can be reframed into:

$$C = \frac{\mathrm{BW}_{\text{3-dB}} \times G_{\text{3-dB}}}{100} \tag{12}$$

Finally, Equation (12) can be expanded for the various components of 3-dB bandwidth and 3-dB gain as:

$$C_1 = \frac{\mathrm{BW}_{\text{3-dB}} \times G_{\text{3-dB(avg)}}}{100} \tag{12a}$$

$$C_2 = \frac{\mathrm{BW}_{\text{3-dB}} \times G_{\text{3-dB(peak)}}}{100} \tag{12b}$$

Hence, the utilization of C_1 and C_2 provides considerable solution to the limitations that are associated with the various available methods of comparison [34]. The conventional approaches compare the CP antennas to single characteristic in practical sense. Here, Equation (12) that is written as the generalized equation (gain-bandwidth product relationship) is described as a study for 1st time in the literature, which is done in

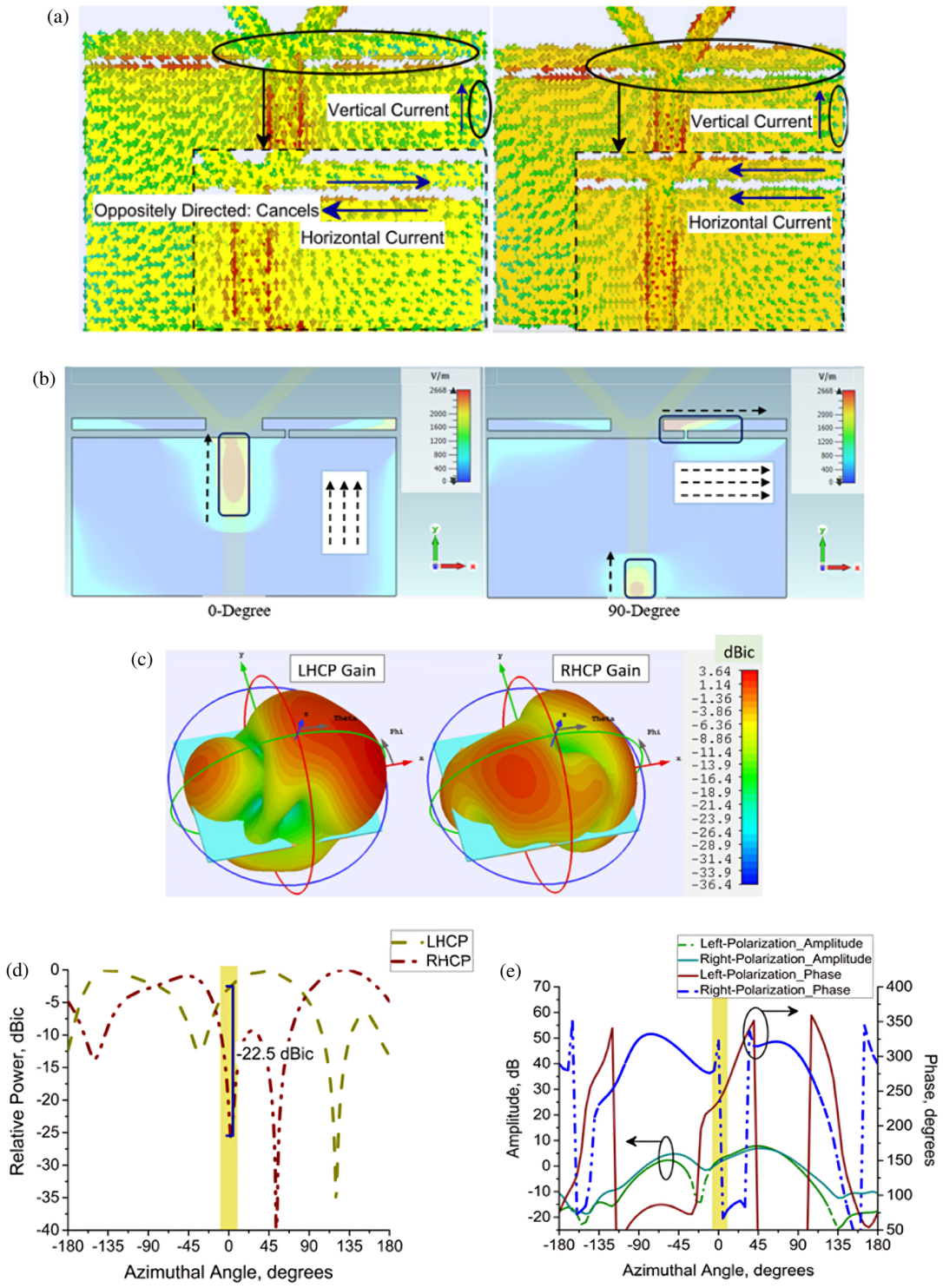

FIGURE 5. Comprehension of CP characteristics at the $f = 5$ GHz: (a) I, (b) II, (c), (d) III; and (e) IV.

order to evaluate the CP antenna. A comparison with the ones that were reported in [10–23] has been included in Table 2 in order to make it more and more relevant. It demonstrates that the proposed SADEA-driven metantenna that was proposed is superior to other printed antennas in the terms of: (a) enhanced bandwidth and (b) gain characteristics. Here, metantenna with a high gain > 8 dBic and good 3-dB beamwidth $> 120°$ will allow for a precise signal concentrating. When it comes to ambient RF energy harvesting/wireless power transmission, the proposed antenna requires precise targeting/situations where the EM signal needs to be carried across the distances with spread &/or receiving from RF signals, considering the fifth-generation and beyond applications [6, 33, 34].

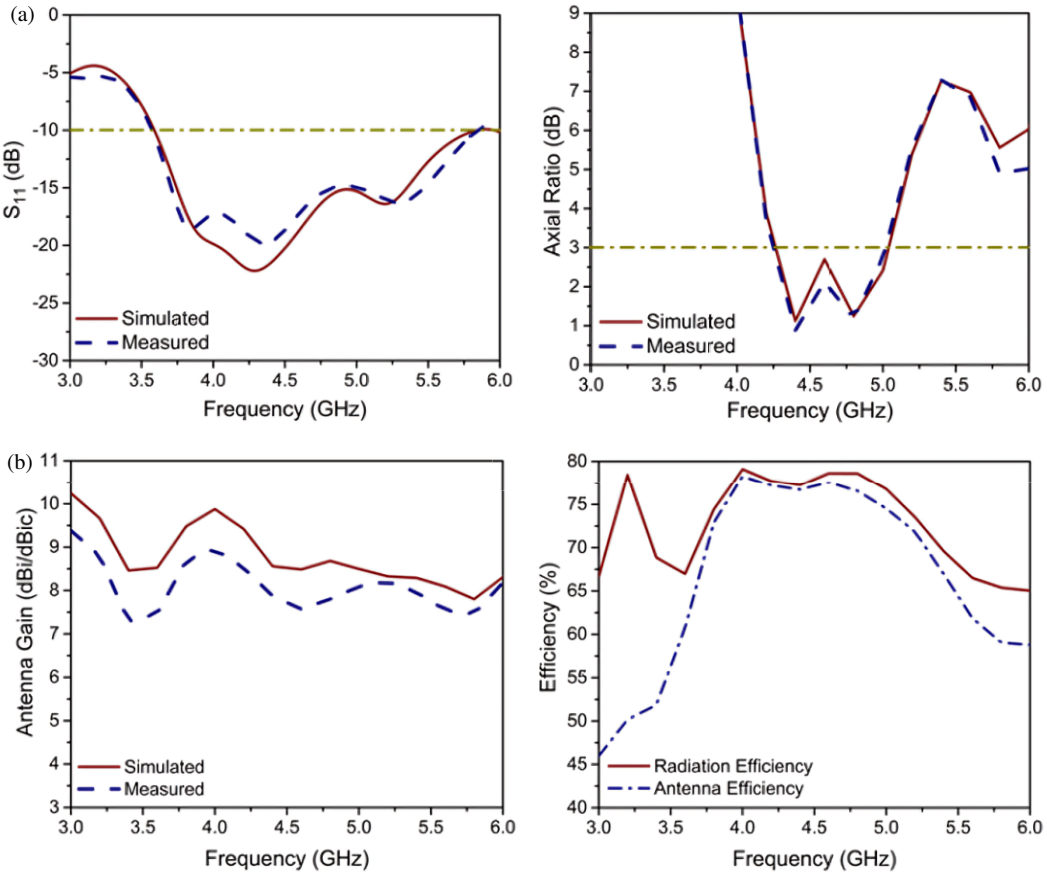

FIGURE 6. Parameters of the metantenna: (a) Bandwidths (IBW, ARBW) and (b) antenna gain & antenna efficiency.

4. PROOF OF CONCEPT TESTING: FABRICATING THE PROTOTYPE AND ITS VALIDATION BY EXPERIMENTATION

Figure 1 highlights the fabricated prototype of proposed CP metantenna using printed circuit board (PCB) prototyping mechanism. The optimized dimensions are presented in Table 1. The simulated and measured IBWs are 2.32 GHz (3.55–5.87 GHz, 49.25%) and 2.35 GHz (3.54–5.89 GHz, 49.84%), respectively, along with the simulated and measured ARBWs of 0.87 GHz (4.24–5.11 GHz, 18.61%) and 0.89 GHz (4.24–5.13 GHz, 18.95%), presented in Figure 6(a). Due to the incorporation of SADEA-tuned metasurface layer (stage-4), simulated & measured antenna gains taken in the average form over the frequency range of 3.5–5.5 GHz lie between 7.48 and 8.85 dBic which is higher, if we consider the conventional printed monopole antenna. It also exhibits an antenna efficiency of $> 70\%$ as shown in Figure 6(b). Based on this outcome, the enhancement in the gain can be correlated with a phase correction, enhanced impedance matching, and reduction of back scattering, where the metasurfaces act as the agent for manipulation of electromagnetic waves. Hence, it optimizes the spatial distribution of the radiated energy, suppresses unwanted backscattering, and sidelobes focusing energies more efficiently in the specified directions. Because of these characteristics, normalized radiation pattern taken at $f = 4.5$ and 5 GHz offers strong directional pattern with front-to-back ratio (FBR) of ≥ -22.5 dBic in its operating band. Hence, SADEA-tuned broadened CP metantenna is investigated for ambient RF energy harvesting/wireless power transmission; so, the attainment of stronger FBRs will be the evaluation regarding the effectiveness of the transmission and reception of EM waves. More specifically, it has positive effects on the antenna's capacity to concentrate on signal coming from the front while reducing interference coming from the back [6, 33, 34]. This fine tuning feature makes the MTS effective for improving efficacy of communication system [35, 36].

In Figures 7(a) and (b), various characteristics associated with radiation are shown. The following observations were made after designing, analyzing, and validating the proposed metantenna reported here as follows:

- A printed monopole antenna and twin parasitic conducting strips (PCSs) are employed with SADEA-tuned metasurface layer acting as a reflector and investigated as a CP metantenna aimed at operating at 5 GHz.

- With the assistance of CEM methodologies, the investigation of CP properties is brought to the forefront. To further introspect the CP features, gain-bandwidth product (GBPR) is utilized.

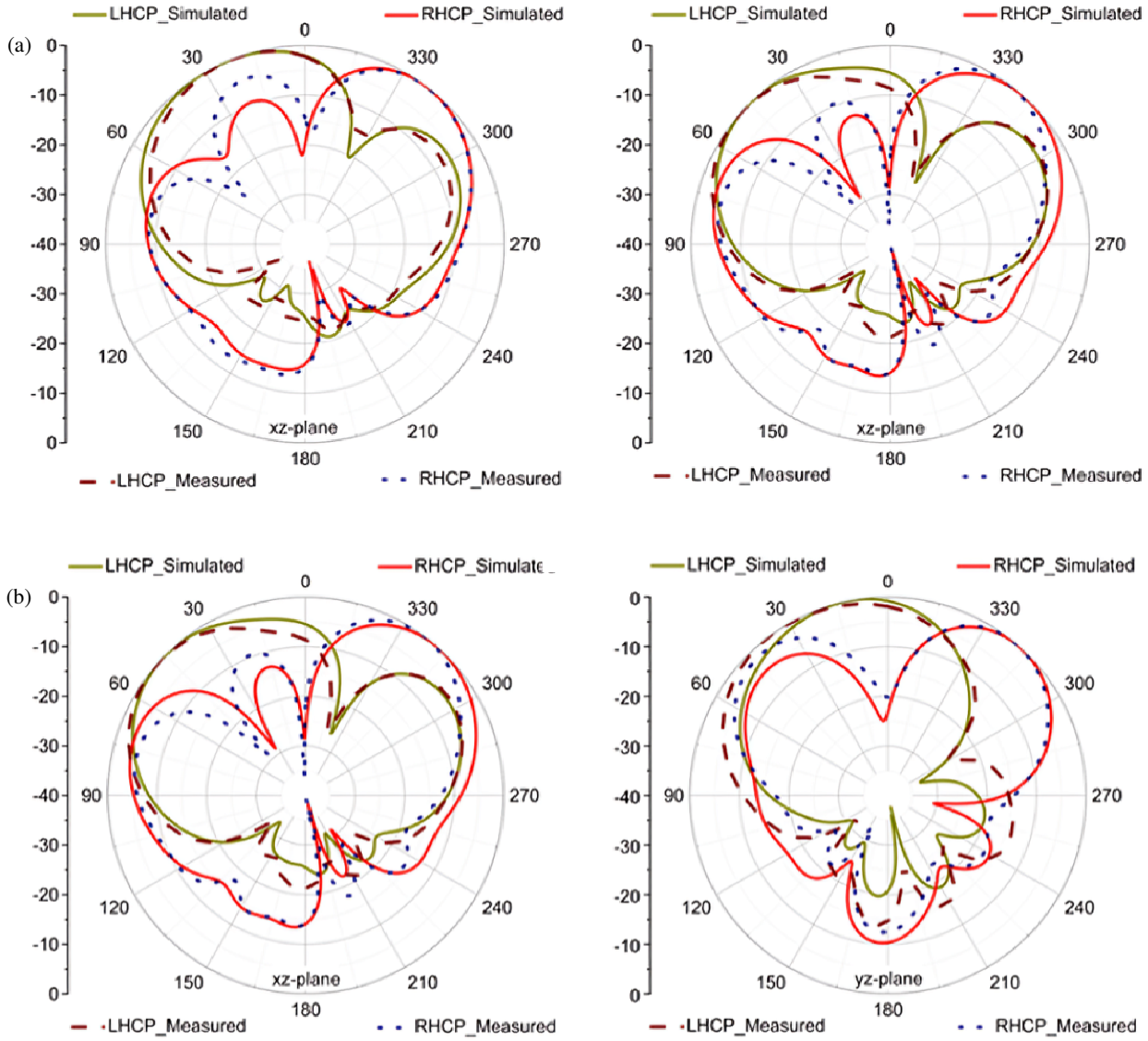

FIGURE 7. Far-field (radiation pattern) properties of the metantenna at: (a) $f = 4.5$ GHz and (b) $f = 5$ GHz.

- Because the metantenna reported in this research has a capability to fulfill the performance trade-offs [34], it evolves for use in the internet-of-things inspired ambient RF energy harvesting/wireless energy harvesting application. The simulation perspective in this regard is presented in the next section.

5. GETTING INSIGHT INTO SIMULATION PERSPECTIVE OF RF ENERGY HARVESTING/WIRELESS ENERGY HARVESTING

Converting background RF signals into DC output is needed for RF energy harvesting. This is done with the incorporation of highly efficient wideband rectifier circuits (GVD) & an impedance matching network (IMN) connected to the RF front-ends. Accordingly [34], the success of the whole system relies on how well the three parts work together as: the RF front ends, impedance matching network (IMN), and rectifier circuit (GVD). To sum up, the main idea is to create a system that can handle the growing power needs of multifunctional electronic parts, as long as RF front ends can balance their performance before being built into circuits. As a result, it should power the sensors in the low-power devices like wearables, medical, & healthcare plug-kits, where they need a steady DC output voltage (V_{out}) from 2.45–5.5 V to work cohesively. Then, a 3-staged Greinacher Voltage Doubler (GVD) in the form of CRLH- and LC-matching rectifier circuit is designed and integrated with a CP metantenna. It is investigated for the input power levels (P_{in}) that range from 0 to +20 dBm, where the obtained V_{out} reaches the maximum limit of 5.76 V and then $\eta_o > 75\%$ at 12 dBm. The corresponding outcomes (DC output voltage, V_{out} and RF-to-DC conversion efficiency, η_o) are superior to the ones that have been reported in the recent works [37–45] and are obtained through the simulation on

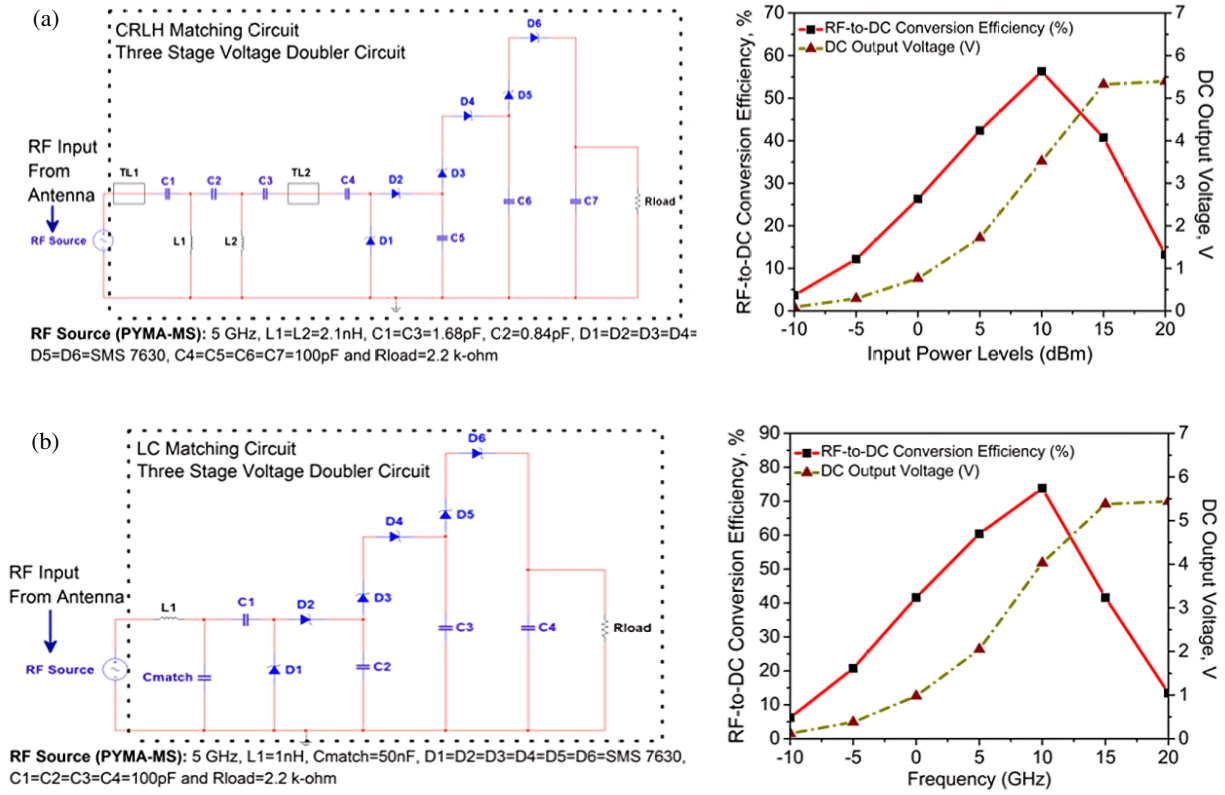

FIGURE 8. Perspective of RF energy harvesting outcomes using metantenna: (a) Circuit-I and (b) Circuit-II.

the ADS platform, with a load resistance of 2.2 kΩ, fixed at the 5 GHz, shown in Figures 8(a) and (b).

6. CONCLUSION

In this research paper, a broadband circularly polarized printed monopole antenna with a high gain driven by SADEA-tuned metasurface acting as a reflector is investigated. It is possible to achieve widened IBW and ARBW, which allows for the CP gain > 8 dBic and antenna efficiency $> 70\%$ in the bands, desired for their operation. Intuition regarding the CP is offered along with its physical insights, with distinct facets grounded in computational electromagnetism (CEM). Further, a comprehensive approach is provided for large-scale remedy to the issue of analyzing CP traits with metantenna, as in the form of gain-bandwidth product relationship (GBR). Then, the attained results are compared with the performance trade-offs derived from [10–23]. Accordingly, this work integrates CEM with SADEA optimization approach powered by a AI, to improve outcomes for meeting the requirements of RF energy harvesting/wireless energy harvesting, and is in line with the growing requirements of applications based on fifth-generation and beyond [2, 34].

REFERENCES

[1] Divakaran, S. K., D. D. Krishna, and Nasimuddin, "RF energy harvesting systems: An overview and design issues," *International Journal of RF and Microwave Computer-Aided Engineering*, Vol. 29, No. 1, e21633, 2019.

[2] Behera, B. R., P. R. Meher, and S. K. Mishra, "Microwave antennas — An intrinsic part of RF energy harvesting systems: A contingent study about its design methodologies and state-of-art technologies in current scenario," *International Journal of RF and Microwave Computer-Aided Engineering*, Vol. 30, No. 5, e22148, 2020.

[3] Toh, B. Y., R. Cahill, and V. F. Fusco, "Understanding and measuring circular polarization," *IEEE Transactions on Education*, Vol. 46, No. 3, 313–318, 2003.

[4] Mishra, S. K., R. K. Gupta, A. Vaidya, and J. Mukherjee, "A compact dual-band fork-shaped monopole antenna for Bluetooth and UWB applications," *IEEE Antennas and Wireless Propagation Letters*, Vol. 10, 627–630, 2011.

[5] Chen, Z. N., X. Qing, W. Liu, H. Sheng, T. Li, and B. Zhang, "Toward metantennas: Metasurface antennas shaping wireless communications," *IEEE Communications Magazine*, Vol. 62, No. 8, 94–99, 2024.

[6] Behera, B. R., P. R. Meher, and S. K. Mishra, "Metasurface superstrate inspired printed monopole antenna for RF energy harvesting application," *Progress In Electromagnetics Research C*, Vol. 110, 119–133, 2021.

[7] Milias, C., R. B. Andersen, P. I. Lazaridis, Z. D. Zaharis, B. Muhammad, J. T. B. Kristensen, A. Mihovska, and D. D. S. Hermansen, "Metamaterial-inspired antennas: A review of the state of the art and future design challenges," *IEEE Access*, Vol. 9, 89 846–89 865, 2021.

[8] Esmail, B. A. F., S. Koziel, and S. Szczepanski, "Overview of planar antenna loading metamaterials for gain performance enhancement: The two decades of progress," *IEEE Access*, Vol. 10, 27 381–27 403, 2022.

[9] Chen, Z. N., X. Qing, Y. Su, and R. Xu, "Toward metantennas: Metamaterial-based antennas for wireless communications," *IEEE Communications Magazine*, Vol. 61, No. 11, 160–165, 2023.

[10] Elahi, M., A. Altaf, Y. Yang, K.-Y. Lee, and K. C. Hwang, "Circularly polarized dielectric resonator antenna with two annular vias," *IEEE Access*, Vol. 9, 41 123–41 128, 2021.

[11] Yue, T., Z. H. Jiang, and D. H. Werner, "Compact, wideband antennas enabled by interdigitated capacitor-loaded metasurfaces," *IEEE Transactions on Antennas and Propagation*, Vol. 64, No. 5, 1595–1606, 2016.

[12] Hussain, N., S. I. Naqvi, W. A. Awan, and T. T. Le, "A metasurface-based wideband bidirectional same-sense circularly polarized antenna," *International Journal of RF and Microwave Computer-Aided Engineering*, Vol. 30, No. 8, e22262, 2020.

[13] Wu, Z., L. Li, Y. Li, and X. Chen, "Metasurface superstrate antenna with wideband circular polarization for satellite communication application," *IEEE Antennas and Wireless Propagation Letters*, Vol. 15, 374–377, 2015.

[14] Chen, Q., H. Zhang, L.-C. Yang, X.-F. Zhang, and Y.-C. Zeng, "Wideband and low axial ratio circularly polarized antenna using AMC-based structure polarization rotation reflective surface," *International Journal of Microwave and Wireless Technologies*, Vol. 10, No. 9, 1058–1064, 2018.

[15] Yang, W., K.-W. Tam, W.-W. Choi, W. Che, and H. T. Hui, "Novel polarization rotation technique based on an artificial magnetic conductor and its application in a low-profile circular polarization antenna," *IEEE Transactions on Antennas and Propagation*, Vol. 62, No. 12, 6206–6216, 2014.

[16] Rajanna, P. K., K. Rudramuni, and K. Kandasamy, "Characteristic mode-based compact circularly polarized metasurface antenna for in-band RCS reduction," *International Journal of Microwave and Wireless Technologies*, Vol. 12, No. 2, 131–137, 2020.

[17] Ameen, M. and R. Chaudhary, "Metamaterial circularly polarized antennas: Integrating an epsilon negative transmission line and single split ring-type resonator," *IEEE Antennas and Propagation Magazine*, Vol. 63, No. 4, 60–77, 2021.

[18] Zheng, Q., C. Guo, and J. Ding, "Wideband and low RCS circularly polarized slot antenna based on polarization conversion of metasurface for satellite communication application," *Microwave and Optical Technology Letters*, Vol. 60, No. 3, 679–685, 2018.

[19] Yang, W., W. Che, H. Jin, W. Feng, and Q. Xue, "A polarization-reconfigurable dipole antenna using polarization rotation AMC structure," *IEEE Transactions on Antennas and Propagation*, Vol. 63, No. 12, 5305–5315, 2015.

[20] Dong, J., C. Ding, and J. Mo, "A low-profile wideband linear-to-circular polarization conversion slot antenna using metasurface," *Materials*, Vol. 13, No. 5, 1164, 2020.

[21] Liu, Y., Y.-X. Huang, Z.-W. Liu, S.-T. Cai, X.-M. Xiong, and J. Guo, "Design of a compact wideband CP metasurface antenna," *International Journal of RF and Microwave Computer-Aided Engineering*, Vol. 30, No. 10, e22332, 2020.

[22] Chen, A. and X. Ning, "A pattern and polarization reconfigurable antenna with metasurface," *International Journal of RF and Microwave Computer-Aided Engineering*, Vol. 31, No. 3, e22312, 2021.

[23] Dong, J., R. Wu, X. Yuan, and J. Mo, "A low-profile broadband circularly polarized metasurface antenna based on characteristic mode analysis," *Waves in Random and Complex Media*, 1–19, 2022.

[24] Grout, V., M. O. Akinsolu, B. Liu, P. I. Lazaridis, K. K. Mistry, and Z. D. Zaharis, "Software solutions for antenna design exploration: A comparison of packages, tools, techniques, and algorithms for various design challenges," *IEEE Antennas and Propagation Magazine*, Vol. 61, No. 3, 48–59, 2019.

[25] Liu, B., H. Aliakbarian, Z. Ma, G. A. E. Vandenbosch, G. Gielen, and P. Excell, "An efficient method for antenna design optimization based on evolutionary computation and machine learning techniques," *IEEE Transactions on Antennas and Propagation*, Vol. 62, No. 1, 7–18, 2014.

[26] Liu, B., S. Koziel, and N. Ali, "SADEA-II: A generalized method for efficient global optimization of antenna design," *Journal of Computational Design and Engineering*, Vol. 4, No. 2, 86–97, 2017.

[27] Liu, B., M. O. Akinsolu, N. Ali, and R. Abd-Alhameed, "Efficient global optimisation of microwave antennas based on a parallel surrogate model-assisted evolutionary algorithm," *IET Microwaves, Antennas & Propagation*, Vol. 13, No. 2, 149–155, 2019.

[28] Akinsolu, M. O., B. Liu, V. Grout, P. I. Lazaridis, M. E. Mognaschi, and P. D. Barba, "A parallel surrogate model assisted evolutionary algorithm for electromagnetic design optimization," *IEEE Transactions on Emerging Topics in Computational Intelligence*, Vol. 3, No. 2, 93–105, 2019.

[29] Liu, B., M. O. Akinsolu, C. Song, Q. Hua, P. Excell, Q. Xu, Y. Huang, and M. A. Imran, "An efficient method for complex antenna design based on a self adaptive surrogate model-assisted optimization technique," *IEEE Transactions on Antennas and Propagation*, Vol. 69, No. 4, 2302–2315, 2021.

[30] Zhang, J., M. O. Akinsolu, B. Liu, and G. A. E. Vandenbosch, "Automatic AI-driven design of mutual coupling reducing topologies for frequency reconfigurable antenna arrays," *IEEE Transactions on Antennas and Propagation*, Vol. 69, No. 3, 1831–1836, 2021.

[31] Zheng, Q., C. Guo, J. Ding, M. O. Akinsolu, B. Liu, and G. A. E. Vandenbosch, "A wideband low-RCS metasurface-inspired circularly polarized slot array based on AI-driven antenna design optimization algorithm," *IEEE Transactions on Antennas and Propagation*, Vol. 70, No. 9, 8584–8589, 2022.

[32] Qiu, Y., Z. Weng, D. Hou, M. Ma, and J. Liu, "Bandwidth enhancement of metasurface antennas by shifting and reshaping high-order mode," *IEEE Antennas and Wireless Propagation Letters*, Vol. 22, No. 4, 933–937, 2023.

[33] Meher, P. R., S. K. Mishra, and M. A. Halimi, "A low-profile compact broadband CP DRA for RF energy harvesting applications," *IETE Journal of Research*, Vol. 70, No. 5, 4540–4548, 2024.

[34] Behera, B., S. Mishra, M. H. Alsharif, P. Uthansakul, and M. Uthansakul, "A metasurface-inspired printed monopole antenna for 5G and RF energy harvesting application," *Engineering Science and Technology, an International Journal*, Vol. 51, 101638, 2024.

[35] Faeghi, P., C. Ghobadi, J. Nourinia, and B. Virdee, "Nanoparticle-coated Vivaldi antenna array for gain enhancement," *Applied Physics A*, Vol. 129, No. 3, 217, 2023.

[36] Shokri, M., P. Faeghi, K. Kaboutari, C. Ghobadi, J. Nourinia, Z. Amiri, and R. Barzegari, "A printed dipole antenna for WLAN applications with anti-interference functionality," in *2021 Photonics & Electromagnetics Research Symposium (PIERS)*, 1486–1494, Hangzhou, China, 2021.

[37] Jie, A. M., Nasimuddin, M. F. Karim, and K. T. Chandrasekaran, "A wide-angle circularly polarized tapered-slit-patch antenna with a compact rectifier for energy-harvesting systems," *IEEE*

Antennas and Propagation Magazine, Vol. 61, No. 2, 94–111, 2019.

[38] Mohd Noor, F. S., Z. Zakaria, H. Lago, and M. A. M. Said, "Dual-band aperture-coupled rectenna for radio frequency energy harvesting," *International Journal of RF and Microwave Computer-Aided Engineering*, Vol. 29, No. 1, e21651, 2019.

[39] Chandrasekaran, K. T., K. Agarwal, Nasimuddin, A. Alphones, R. Mittra, and M. F. Karim, "Compact dual-band metamaterial-based high-efficiency rectenna: An application for ambient electromagnetic energy harvesting," *IEEE Antennas and Propagation Magazine*, Vol. 62, No. 3, 18–29, 2020.

[40] Surender, D., M. A. Halimi, T. Khan, F. A. Talukdar, and Y. M. M. Antar, "Circularly polarized DR-rectenna for 5G and Wi-Fi bands RF energy harvesting in smart city applications," *IETE Technical Review*, Vol. 39, No. 4, 880–893, 2022.

[41] Halimi, M. A., T. Khan, A. A. Kishk, and Y. M. M. Antar, "Efficient rectifier circuit operating at N78 and N79 sub-6 GHz 5G bands for microwave energy-harvesting and power transfer applications," *International Journal of Microwave and Wireless Technologies*, Vol. 16, No. 1, 75–82, 2024.

[42] Bougas, I. D., M. S. Papadopoulou, A. D. Boursianis, S. Nikolaidis, and S. K. Goudos, "Dual-band rectifier circuit design for IoT communication in 5G systems," *Technologies*, Vol. 11, No. 2, 34, 2023.

[43] Yue, Z., X. Xu, S. Li, X. Q. Lin, L. J. Zhong, and M. D. Shi, "Design of efficient and compact ultrawideband rectifier for sub-6 GHz WPT/EH," *IEEE Microwave and Wireless Technology Letters*, Vol. 33, No. 10, 1490–1493, 2023.

[44] Kong, Y., X. Bai, L. Xu, and J. Chen, "High-efficiency 5G-band rectifier with impedance dispersion compensation network," *Electronics*, Vol. 13, No. 16, 3105, 2024.

[45] Gyawali, B., M. Aboualalaa, A. Barakat, and R. K. Pokharel, "Design of miniaturized sub-6 GHz rectifier with self-impedance matching technique," *IEEE Transactions on Circuits and Systems I: Regular Papers*, Vol. 71, No. 7, 3413–3422, 2024.